



In-situ real-time and ex-situ spectroscopic analysis of Al₂O₃ films prepared by plasma enhanced atomic layer deposition

Running title: JVB19-AR-ICSE2019-00313R

Running Authors: Johanna Reck

Franziska Naumann¹, Johanna Reck^{1a}, Hassan Gargouri¹, Bernd Gruska¹, Adrian Blümich², Ali Mahmoodinezhad³, Christoph Janowitz³, Karsten Henkel³, Jan Ingo Flege³

¹SENTECH Instruments GmbH, Schwarzschildstraße 2, 12489 Berlin, Germany

²AEMtec GmbH, James-Franck-Str. 10, 12489 Berlin, Germany

³Brandenburg University of Technology Cottbus-Senftenberg, Applied Physics and Semiconductor Spectroscopy, K.-Zuse-Str. 1, 03046 Cottbus, Germany

a) Electronic mail: johanna.reck@sentech.de

In-situ real-time ellipsometry (irtE) with a very high time resolution of 24 ms was applied to monitor the inductively coupled plasma-enhanced (ICPE) atomic layer deposition (ALD) process of Al₂O₃ thin films to precisely resolve each step of the ALD process and its complete cycle. The influences of plasma power, plasma pulse duration, and deposition temperature on the film growth characteristics were investigated. Ex-situ ellipsometry (UV-VIS-NIR-SE and IR-SE) and X-ray photoelectron spectroscopy (XPS) revealed the bulk properties (thickness, refractive index, chemical composition, and carbon incorporation) of the films, which together with the in-situ results are compared to those of films prepared by thermal ALD (T-ALD).

The ICPEALD films were deposited at substrate temperatures between 80 and 250 °C; the role of plasma power (50 – 300 W) and its pulse duration (1 – 20 s) were investigated at 250 °C. The reference T-ALD layers were prepared at 200 °C. The ICPEALD process of Al₂O₃ shows an increased growth rate, and the produced films

exhibit higher carbon contaminations compared to T-ALD Al_2O_3 films. Plasma pulse times up to 15 s further increase the content of carbon and CH-species; at the same time the refractive index decreases. The optical properties of ICPEALD deposited Al_2O_3 films are comparable with those of T-ALD films for low plasma power and short plasma pulse durations. For the ICPEALD films UV absorption is found; it is dependent on the deposition parameters. IrTE resolves process effects that correlate to bulk properties of Al_2O_3 such as impurities as well as oxygen deficiencies.

I. INTRODUCTION

Atomic layer deposition (ALD) is a chemical gas phase deposition method based on substrate surface reactions. The fast-developing technique for thin film deposition for a variety of applications is different to other deposition techniques; in ALD gaseous precursors are pulsed into the reactor chamber alternately, separated by purging periods. By exposing the precursors to the modified substrate surface repeatedly, a thin film is deposited monolayer by monolayer. This deposition technique offers a unique self-limiting film growth mechanism allowing thickness control on an atomic scale. The outstanding properties of ALD such as high conformity on high aspect structures, high uniformity, and pin-hole free growth are beneficially used in several applications requiring thin film depositions.¹⁻⁶

ALD is receiving attention especially for its potential applications in advanced high-k dielectrics such as Al_2O_3 , HfO_2 , etc. Thin aluminum oxide (Al_2O_3) layers deposited by ALD have been applied in energy conversion and microelectronic

devices.^{3,7-19} In particular, effects such as surface passivation or encapsulation in photovoltaic devices,^{3,7,20} interfacial buffering for high-k dielectrics,^{8,9} organic memories,¹⁰ and nanolaminates,¹¹ work function modification,¹² or gas diffusion limitation¹³ can be used to improve device performance.

The typical precursors for thermal ALD (T-ALD) of Al₂O₃ are trimethylaluminium (TMA) as aluminum source and water as oxygen source.^{2,3,21} In plasma-enhanced ALD (PEALD), water is replaced by an oxygen plasma,^{3,4,21} which extends the capabilities of ALD in improved film quality and increased flexibility in process conditions.^{4,21} PEALD is preferred instead of T-ALD for the deposition at low temperatures, allowing the coating of organic semiconductor devices and thermally fragile substrates.^{2,4,7,13} There are different types of plasma sources for PEALD such as “true remote capacitively coupled plasma source” (referred to as PEALD in the following)²² and inductively coupled plasma source (henceforth referred to as ICPEALD)²³. In the former, the substrate does not directly make contact with the plasma, which is the main difference between the two techniques.

Optimizing the 4-phase cycle of ALD is essential but can be time-consuming and expensive if ex-situ analysis is available only. The monitoring of the ALD process in real-time allows investigating the crucial growth mechanisms of T-ALD and ICPEALD to optimize each of the 4 phases of the ALD cycles directly during deposition.

Here, we compare Al₂O₃ films that were deposited by T-ALD as well as by ICPEALD. In-situ real-time ellipsometry (irtE) was used to monitor the ICPEALD process of Al₂O₃ films. A high measurement speed of 24 ms and a high signal to noise ratio (resolution of $\delta\Delta = 0.1^\circ$) enable the characterization of surface processes within each phase of an ALD cycle, in particular the precursor adsorption and the surface reactions during the plasma pulse.

Our work focuses on the relationship between ellipsometric in-situ real-time measurements during the ALD of Al₂O₃ layers and the ex-situ determined properties of these layers. Ex-situ spectroscopic ellipsometry in the deep ultraviolet and visible (DUV-VIS) and in the mid infrared (MIR) spectral ranges as well as XPS measurements were performed on 100 nm thick Al₂O₃ films to determine the optical properties and the chemical composition of the bulk material.

The results of ICPEALD Al₂O₃ films are compared to those of T-ALD Al₂O₃ films. As a main result, irtE shows a correlation between growth effects and bulk properties of the Al₂O₃ films.

II. EXPERIMENTAL

EXPERIMENTAL SETUP

Al₂O₃ ALD layers were prepared in the SENTECH atomic layer deposition system. The deposition tool was equipped with a load-lock for clean and reliable processing and an in-situ real-time ellipsometer (SENTECH ALD Real Time Monitor, ALD-RTM) for an in-situ, non-destructive real-time monitoring of the deposition process.



The ALD system enables thermal and plasma enhanced deposition. For plasma enhanced deposition, a planar triple spiral antenna (PTSA 200) is used as inductively coupled plasma (ICP) source mounted on top of the reactor chamber. This way, we are able to process the samples in the same chamber, avoiding the possibly detrimental influence of utilizing different ALD systems and in-situ measurement systems. TMA as well as H₂O for the T-ALD and O₂ for the ICPEALD as co-reactants were used as precursor of aluminum and oxygen, respectively. Simultaneously, high-purity nitrogen (N₂, 99.999%) was used as carrier and purge gas with gas pressure at 12 Pa during the whole ALD process. In ICPEALD, 80 °C, 150 °C, and 250 °C were used as deposition temperatures, whereas in T-ALD 200°C was applied.

TMA and H₂O were alternately pulsed in the N₂ carrier flow using gas switching valves. After each 60 ms precursor phase a 2 s purge phase was applied, which results in a total T-ALD cycle time of 4.12 s. The ICPEALD cycle times were varied according to the parameters listed in Table 1.

TABLE 1: ICPEALD- and T-ALD-process parameters

Process parameters	ICPEALD	T-ALD
1 st precursor		TMA
Co-reactant	O ₂	H ₂ O
Carrier gas		Nitrogen (N ₂)
TMA pulse [ms]	60	60
TMA purge [s]	20	2
Co-reactant pulse (t _{CR}) [s]	1, 2, 5, 15, 20	0.060
2 nd purge [s]	20	2
Deposition temperature [°C]	80, 150, 250	200
Plasma power (P _p) [W]	50, 100, 150, 200, 300	-
Total pressure (P)	12.8 Pa	12 Pa

4" silicon wafers of 525 ± 25 μm thickness and resistivity of 1-10 $\Omega \cdot \text{cm}$ were used as substrates for the Al_2O_3 film depositions. A 4 nm thick Al_2O_3 film was deposited by T-ALD before starting experiments to suppress the interaction with the silicon substrate and to ensure a linear growth of the films.

For in-situ analysis, five cycles were carried out; cycles two to four were averaged for the characterization. For ex-situ analysis, ~ 100 nm thick films were grown by T-ALD and ICPEALD. The T-ALD film thickness was 50 nm for the XPS analysis, measured by irtE. The growth per cycle (GPC) was calculated by dividing the ex-situ determined film thickness by the number of cycles.

CHARACTERIZATION AND MEASUREMENT METHODS

A. *In-situ ellipsometry*

The in-situ real-time ellipsometer allows monitoring the short ALD cycles (typ. a few seconds) with high time resolution (24 ms) and a very high signal to noise ratio ($\delta\Delta = 0.01^\circ$, Δ ellipsometric angle) at a single wavelength of 632.8 nm at 70° angle of incidence. Start and end of the pulse / purge times were transferred from the ALD instrument to the ellipsometer, facilitating the recording of typical ellipsometric data, as, e.g., Ψ (amplitude component) and Δ (phase shifts), in a time-resolved manner.

B. *Ex-situ ellipsometry*

The optical properties of 100 nm thick Al_2O_3 films were investigated by spectroscopic ellipsometry in different spectral ranges. UV/VIS/NIR measurements were

performed with a SENTECH SER 850 in wavelength range from 200 to 1000 nm at two angles of incidence, i.e., at 65° and 70°. The measured spectra were fitted assuming a single layer described by a single Tauc-Lorentz oscillator²⁴ and variable film thickness.

IR spectra from 400 cm⁻¹ to 6600 cm⁻¹ (1,500 nm – 25,000 nm) were measured at an incident angle of 65° using a SENTECH SENDIRA IR ellipsometer. Molecular vibrational bands were extracted and correlated to XPS results.

C. XPS measurements

Laboratory-based X-ray photoelectron spectroscopy (XPS) was carried out on selected samples (refer to Table III) using a hemispherical analyzer (Omicron EA 125) as well as Al K α (1486.6 eV) and Mg K α (1253.6 eV) excitation. The photoelectrons were collected at a take-off angle of 90° with respect to the surface plane to investigate the deeper layers rather than the topmost layer, which is strongly sensitive to surface contamination. To remove surface contamination, the sample surface was cleaned by Ar⁺ sputtering (2 keV, 4 x 10⁻⁶ mbar) for one minute applying an ISE 5 Cold Cathode Ion Sputter Source (Scienta Omicron). The elemental contributions and the aluminum to oxygen (Al:O) ratio were calculated by weighting the fitted XPS core-level intensities, taking into account the respective atomic cross sections and transmission factors of the analyzer.²⁵ The latter were determined by analyzing a single crystal of known elemental contribution after cleaving under UHV conditions in two different modes of operating the hemispherical analyzer, i.e., constant analyzer energy and constant retarding ratio, for both photon energies (Al K α and Mg K α), in accordance with Ref. 25.

III. RESULTS AND DISCUSSION

A. *In-situ-characterization*

The change in polarization of the amplitude ratio Ψ , and the phase Δ during the surface reaction is measured as a function of process time (Fig. 1). Changes of the phase Δ ($\delta\Delta$ – relative delta) correlated to film growing processes and indicated precise surface reactions without the need of modelling. During the deposition process each individual step of an ALD cycle was monitored by the irtE-system. These steps are exemplarily shown for the T-ALD process in Fig. 1 where they are displayed with different colors. The start of the TMA pulse (Step #1) induced a sharp $\delta\Delta$ (black, x) decrease. This indicates an increase in film thickness induced by the precursor adsorption on the substrate surface. While purging (to get rid of the TMA excess and the reaction product CH_4) with nitrogen (Step #2), $\delta\Delta$ (red, \square) remained constant, and no surface change could be detected in this step. During the water pulse (Step #3), $\delta\Delta$ (green, \circ) increased sharply and saturated after a few ms according to the ligand removal. The purging after H_2O pulsing (Step #4) caused no changes in $\delta\Delta$ (blue, \triangleleft). The irtE high time resolution of 24 ms is also displayed in Fig. 1 (inset figure).

We assumed that the process was saturated and self-limited when the delta signal stopped changing and remained stable. To ensure a self-limited surface reaction, long pulsing lengths were chosen for all ALD reaction cycles.

Both, the film thickness and refractive index changed during the growth process and its optimization. Therefore, these parameters cannot reliably be determined at the same time for such thin films, e.g. a few nanometer thick films. At the applied wavelength of 632.8 nm, the films are transparent for all process parameter variations,

and we assumed a negligible roughness. It should be clarified here that the aim of this signal analysis is the process optimization.

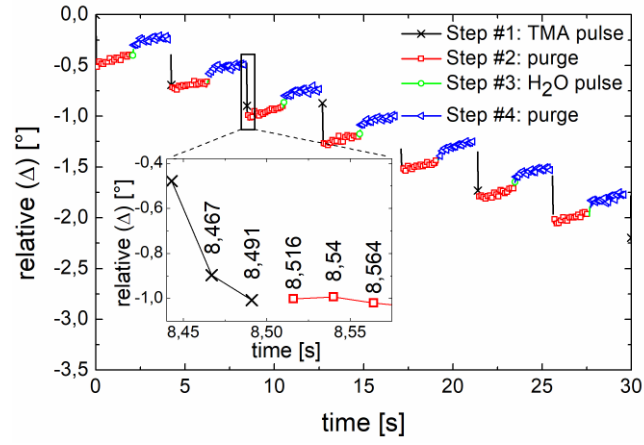


Fig. 1. In-situ real-time ellipsometer Δ -signal changes ($\delta\Delta$) during a T-ALD process of Al_2O_3 (the deposition parameters are given in Table I). The changes correlate with film thickness changes and reveal a linear film growth resolving each cycle steps with high time resolution of 24 ms (inset figure).

Figure 2 shows time-dependent Δ -changes for the ICPEALD growth of Al_2O_3 films for different plasma pulse durations (Fig. 2a) and different plasma powers (Fig 2b). After an instantaneous increase of the $\delta\Delta$ value induced by the plasma pulse (according to Step #3) a fast saturation of the process would be expected. Instead, for longer plasma pulses and high plasma powers an unintentional decrease of $\delta\Delta$ was observed (see detailed views in Fig. 3).

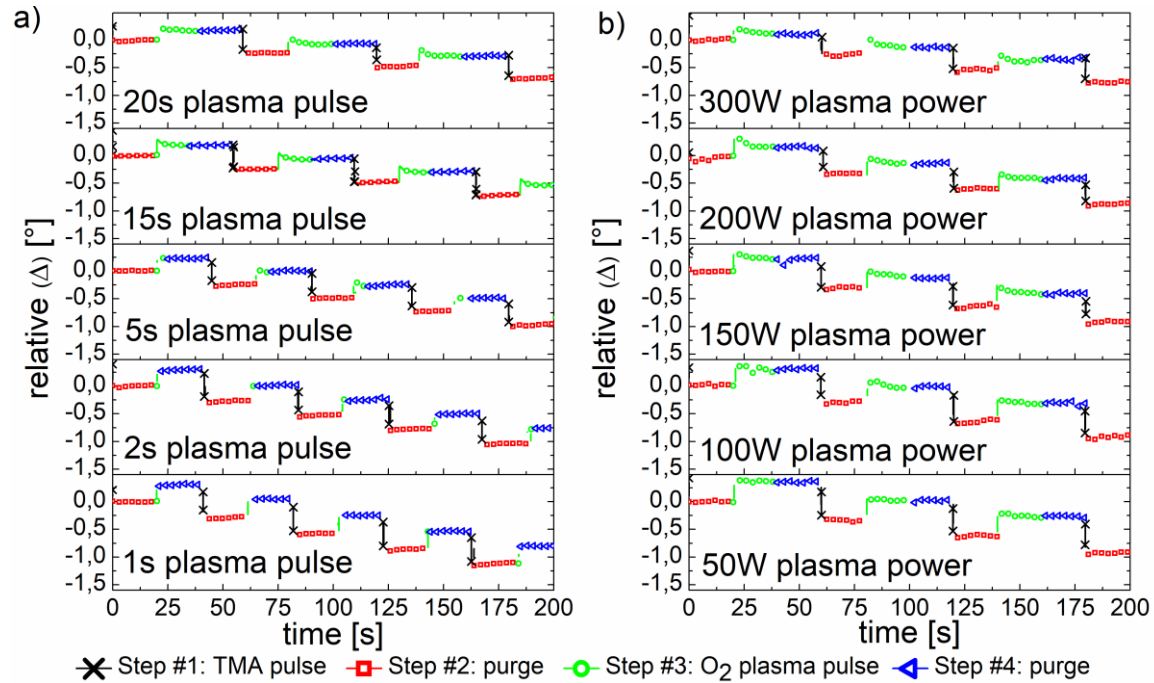


Fig. 2. $\delta\Delta$ vs. ALD process time for different a) plasma pulse durations (1 s, 2 s, 5 s, 15 s, 20 s at $P_p=200$ W) and b) plasma powers (50 W, 100 W, 150 W, 200 W, 300 W at $t_{CR}=15$ s) of ICPEALD Al_2O_3 films deposited at 250 °C. The other fixed process parameters are given in Table I.

Figure 3 shows exemplarily details of selected situations of Fig. 2 illustrating the significant differences within one ICPEALD process cycle. Long ICP pulses (e.g. 15 s) induced a $\delta\Delta$ -decrease followed by a saturation effect after seconds (Fig. 3a, labeled as “unintentional adsorption”). We interpret this unintentional adsorption as a further surface / film change although the process is supposed to be self-limiting. In contrast, short ICP pulses (e.g. 1 s) and T-ALD processes did not show this effect. A much lower $\delta\Delta$ induced by the TMA pulse (Step # 1) was observed for longer ICP pulses (see Fig. 3a -labeled by “less TMA adsorption”- and 4a). A similar effect can be observed when the plasma power is increased (see Fig. 3b and Fig. 4b).

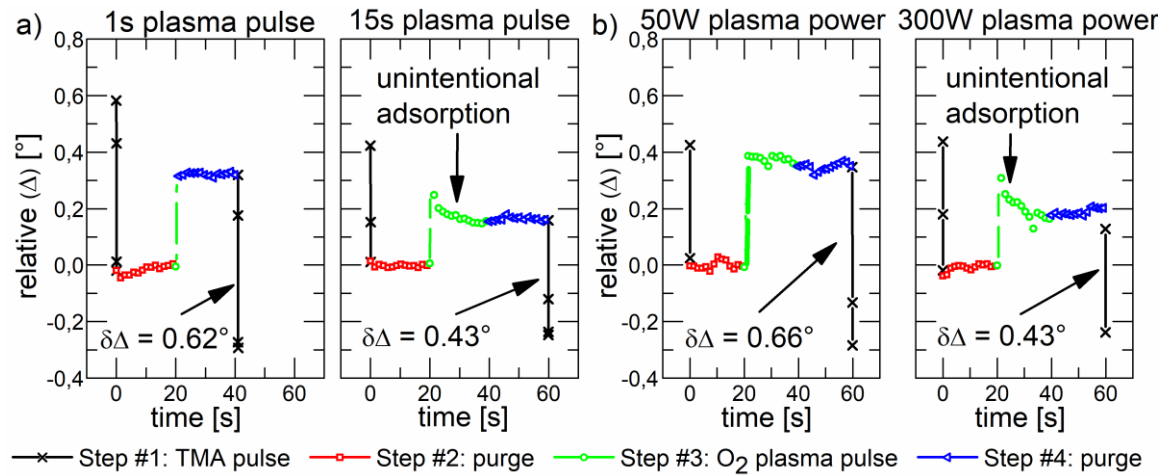


Fig. 3. Comparison of $\delta\Delta$ in dependence of different a) plasma pulse durations (1 s left, 15 s right at $P_p = 200$ W) and b) plasma powers (50 W left, 300 W right at $t_{CR} = 20$ s) of ICPEALD Al₂O₃ films deposited at 250 °C.

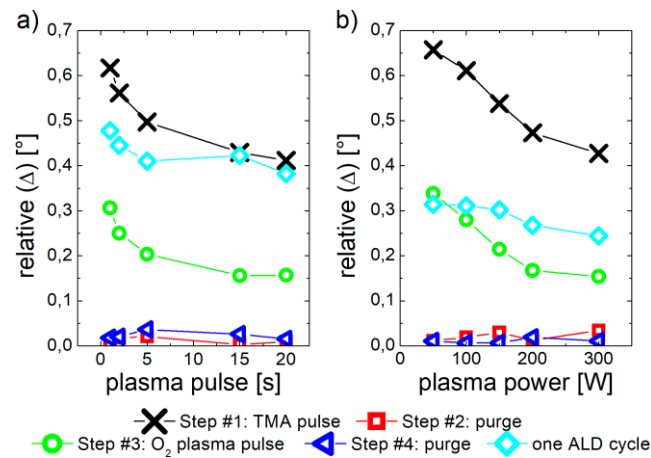


Fig. 4. Comparison of $\delta\Delta$ in dependence of a) plasma pulse duration (at $P_p = 200$ W) and b) plasma power (at $t_{CR} = 20$ s) of ICPEALD Al₂O₃ films deposited at 250 °C showing an unintentional decrease during O₂ plasma pulse (Step #3, green open circles) and a lower TMA reaction (Step #1, black, x) inducing a reduced $\delta\Delta$ for the whole ALD cycle (turquoise, \diamond).

To investigate the influence of deposition temperature, two fixed combinations of deposition parameters were chosen. The plasma pulse length was selected to be either 1 s

(Fig. 5a) or 15 s (Fig. 5b), at 200 W plasma power. The comparison of these dependences unveiled systematic differences of the film deposition behavior for the TMA (Step #1) and plasma pulses (Step #3), with trends of an amplified increase in $\delta\Delta$ with increasing deposition temperature. The different plasma pulse lengths induced different levels of $\delta\Delta$ of Step #1 where a plasma pulse duration of 15 s revealed a much lower $\delta\Delta$.

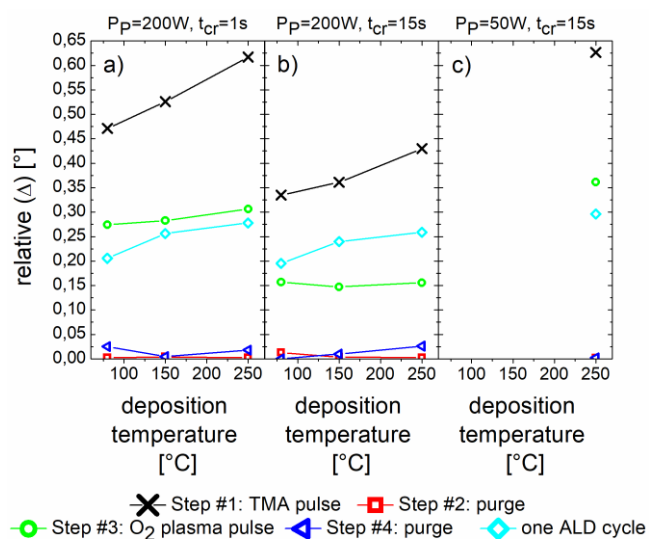


Fig. 5. Comparison of $\delta\Delta$ for the 4-phases of the ALD cycles in dependence of deposition temperature for a) $t_{cr} = 1$ s, $P_p = 200$ W; b) $t_{cr} = 15$ s, $P_p = 200$ W; and c) $t_{cr} = 15$ s, $P_p = 50$ W.

Different levels of $\delta\Delta$ were also detected for the plasma pulse (Step #3) when comparing these two differently prepared sample series although a strong trend with temperature was not detected. For short plasma pulse lengths, a slight increase of $\delta\Delta$ can be recognized for increased deposition temperatures (Fig. 5a).

While the $\delta\Delta$ during the TMA pulse is related to adsorption, the $\delta\Delta$ of the plasma pulse is in the opposite direction and induces a change of surface due to desorption

(compare to Fig. 3). The reduction of the plasma power increased the $\delta\Delta$ (for long plasma pulse lengths) as additionally shown in Fig. 5c. Noteworthy, the ICPEALD samples ($t_{cr} = 15$ s, $P_p = 50$ W) and ($t_{cr} = 1$ s, $P_p = 200$ W) show almost the same $\delta\Delta$ during the ALD process Step #1. TMA and plasma pulses (Steps #1 and #3) were optimized to achieve saturation of the reaction on the substrate surface. The GPC was then constant and did not change with longer plasma pulse duration. To avoid the CVD regime, the purge time between TMA and plasma pulses (Steps #2 and #4) had to be optimized as well.²⁶ To study the effect of plasma power and plasma pulse duration on the chemical composition of aluminum oxide films, MIR ellipsometry and XPS analysis were carried out.

B. Ex-situ measurements

1. Spectroscopic ellipsometry

The ex-situ measured and fitted spectral ellipsometric (Ψ , Δ)-spectra of ~ 100 nm thick films are very similar for all samples, exemplarily shown in Fig. 6. The film thickness, as a result of the fitting procedure of the (Ψ , Δ)-spectra (listed in Table II), and the number of cycles were used to calculate the growth per cycle value (c.f. Fig. 8 a).

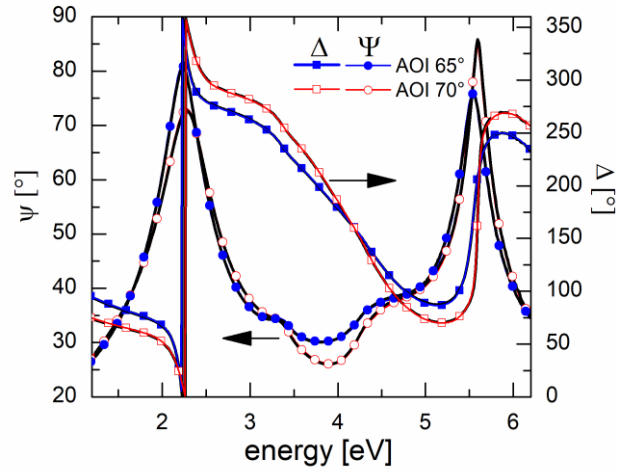


Fig. 6. Measured (black solid line) and fitted Ψ and Δ spectra for 65° and 70° angle of incidences for a 104 nm thick Al_2O_3 film deposited by ICPEALD at 250 °C ($P_p=50$ W, $t_{CR}=15$ s). In contrast to the given values in Table I, here the TMA and plasma purge durations were 5 s and 1 s, respectively).

TABLE II: Determined film thicknesses of the films resulting from fitting (Ψ , Δ)-spectra. For the ICPEALD samples the substrate temperature, P_p and t_{CR} are given.

Sample	d [nm]
T-ALD (200 °C)	100.4 ± 0.1
ICPEALD (80 °C, 200 W, 15 s)	103.4 ± 0.1
ICPEALD (80 °C, 200 W, 1 s)	104.4 ± 0.1
ICPEALD (150 °C, 200 W, 15 s)	104.6 ± 0.1
ICPEALD (150 °C, 200 W, 1 s)	101.6 ± 0.1
ICPEALD (250 °C, 200 W, 15 s)	105.7 ± 0.1
ICPEALD (250 °C, 200 W, 1 s)	99,8 ± 0.1
ICPEALD (250 °C, 50 W , 15 s)	100.3 ± 0.1

The spectral refractive index (Fig. 7a) and extinction coefficient (Fig. 7b) were extracted from the spectroscopic ellipsometry analysis as well. For short plasma pulses ($P_p=200\text{W}$, $t_{cr}=1\text{ s}$) or low plasma power ($P_p=50\text{ W}$, $t_{cr}=15\text{ s}$) at high deposition temperatures, the refractive index is in very good agreement with the refractive index of the T-ALD films for the complete spectral range. On the other hand, the spectral refractive index reduces drastically with higher temperatures when high power and long plasma pulse durations are used.

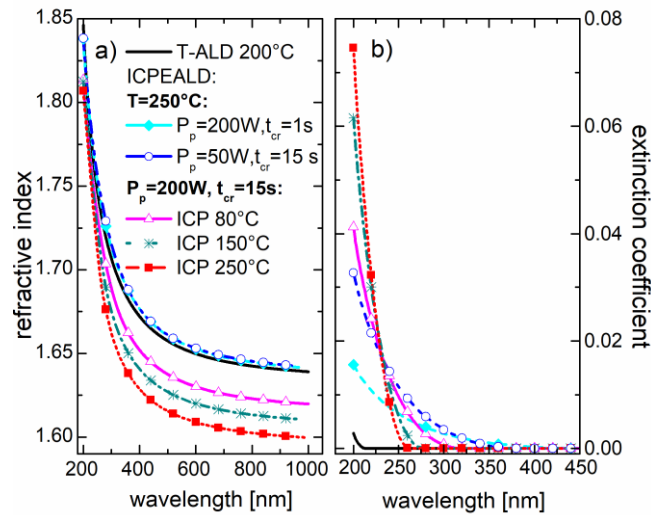


Fig. 7. Refractive index and extinction coefficient for differently deposited, $\sim 100\text{ nm}$ thick Al₂O₃ films.

Films prepared by ICPEALD showed a larger extinction coefficient in the UV spectral range when compared to T-ALD films (Fig. 7b). Even for short ICP plasma pulses and low plasma power it is obvious that the film quality differs from that of the T-ALD Al₂O₃ film. The latter one has a typical onset of the extinction coefficient at ~ 210

nm or lower. For all ICPEALD samples this onset is far above 210 nm in wavelength. Increasing deposition temperatures during the application of long plasma pulses (e.g. 15 s) in the ICPEALD process shift this absorption towards the UV range but increase the total absorption.

Qualitatively different absorption behavior was found for high plasma power and short plasma pulse times ($P_p=200$ W, $t_{CR}=1$ s) as well as for reduced plasma power and long pulses ($P_p=50$ W, $t_{CR}=15$ s) as displayed by the cyan diamonds and blue circles in Fig. 7b. The smaller increase at shorter wavelengths but the onset at longer wavelengths indicate a different reason for the absorption and cannot be explained by composition effects. To model this onset neither a Cauchy model nor a Sellmeier model is applicable. Since the ALD derived films were amorphous, the Tauc-Lorentz model was chosen for modeling the measured (Ψ , Δ) spectra. This model is consistent with the Kramers-Kronig relation and ensures complete transparency for the VIS spectral range.³¹

To emphasize that this absorption is not band gap related we did not use a Tauc plot to estimate the absorption onset. Rather, the values given in Fig. 8b were taken as pure values of the Tauc-Lorentz model and only deliver the information where the absorption of the films starts. Ex-situ ellipsometry revealed that the refractive index clearly depends on plasma pulse duration and deposition temperature (Fig. 8c).

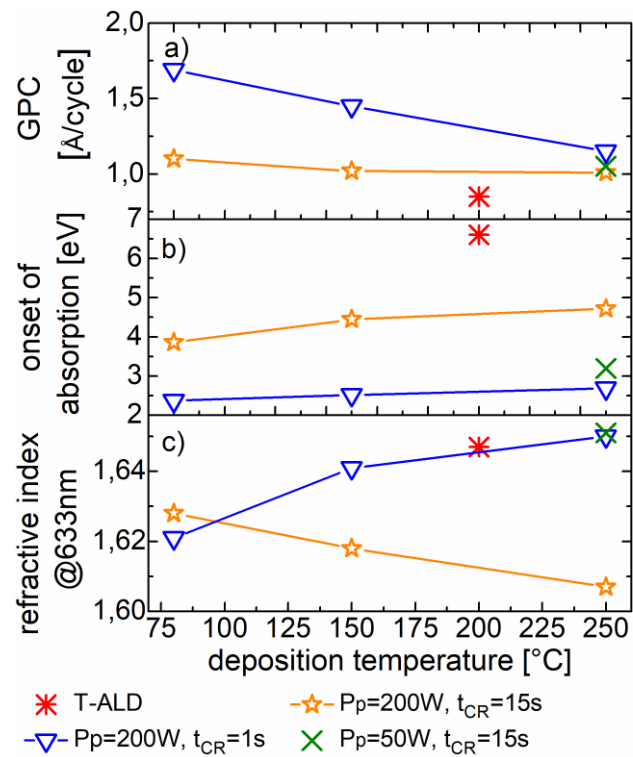


Fig. 8. Calculated GPC values (a) as well as results of (Ψ , Δ)-spectra fitting such as (b) onset of absorption and (c) refractive index (n) in dependence of deposition temperature for different plasma powers and co-reactant pulse times as given in the legend.

IR ellipsometry spectra (Fig. 9) show the Al-O band at 600 cm^{-1} and the Si-O LO band of the substrate at 1250 cm^{-1} for all measured samples. A shifted Al-O LO stretching band towards lower wavenumbers (see Fig. 9a) and additional vibration modes (Fig. 9b) were recorded in the infrared spectra of the ICPEALD grown films depending on temperature and plasma pulse lengths, particularly for low temperature on the one hand or high plasma power in combination with a long plasma pulse on the other hand. In contrast, for increasing temperatures and short plasma pulse length (e.g. $t_{\text{CR}}=1\text{ s}$) as well

as decreased power (e.g. $P_p=50$ W) the Al-O mode became stronger and was close to the reference mode of the T-ALD film (refer to Fig. 9a).

The additional vibration modes in the spectral range above 1200 cm^{-1} (Fig. 9b) can be correlated to different carbon bonds caused by carbon incorporation. The incorporation of CH and CO modes was increased with higher ICP power and longer ICP pulse time. The CH_3 , CO and CH modes were observed at ~ 1250 cm^{-1} , ~ 1500 cm^{-1} , ~ 1350 cm^{-1} , respectively. For lower temperatures the composition was different and no CH mode vibrations were detected at ~ 1300 cm^{-1} . CO modes only remained for short plasma pulse lengths and were reduced by temperature increase. In addition, the absorption mode found at ~ 3500 cm^{-1} (data not shown) remained visible for longer plasma purge times even at lower temperatures. This was caused either by a CH band or even an OH band. These different types of carbon incorporation are the reason for the decrease of the refractive index at the respective deposition parameters.¹³

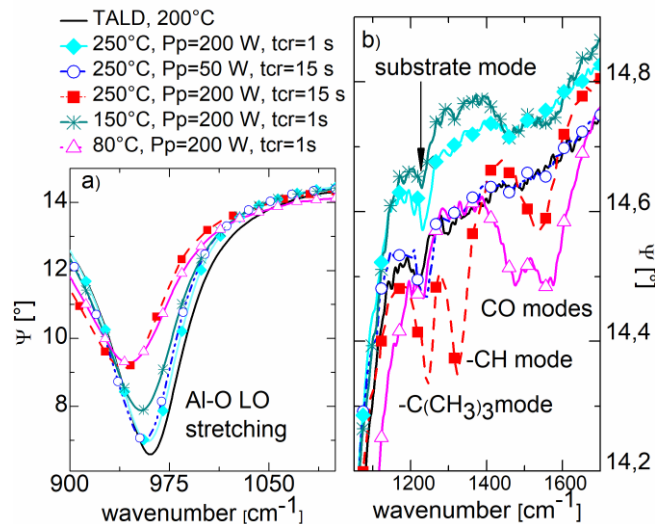


Fig. 9. IR spectra of T-ALD and ICPEALD grown Al_2O_3 films depict Al-O LO stretching band (a) and various carbon vibration modes (b).

2. XPS characterization

Selected samples prepared in different ALD processes were characterized by XPS. The Al2p, O1s, and C1s core levels were recorded to determine the Al:O ratio and also the carbon concentration of the differently prepared films. The XPS survey data resolved relevant photoelectron peaks (Al, O) as well as C 1s signals for the as-deposited samples. Most likely, carbon contamination was significantly enhanced when the samples were exposed to ambient conditions during the transfer for ex situ XPS analysis. The presence of carbon affects particularly the elemental contribution and ratio. Hence, the samples were sputtered by Ar⁺ ions to obtain the bulk composition. The atomic Al:O ratio of the grown layers was determined using Mg K α radiation because at this excitation energy the O1s core level region shows a single photoelectron peak without disturbing contributions of satellites or Auger lines. Notably, after Ar⁺ sputtering the Al:O ratio is close to the expected stoichiometric value of 2:3 for the T-ALD Al₂O₃ thin films. In comparison, a slight reduction to 0.62 is found for the ICPEALD sample (see Table III).

For the determination of the carbon content within the films the C1s spectra were recorded using Al K α excitation; neither Auger nor satellite lines are found (in contrast to Mg K α excitation) in this energy region. The carbon concentration is 8.8 ± 0.1 % for the T-ALD (200 °C) whereas for the ICPEALD sample the value is distinctly increased (see Table III). The data of this XPS analysis are summarized in Table III. For comparison with our previous results on T-ALD Al₂O₃ films²⁷, XPS spectra were also recorded for the as-grown samples yielding a very good agreement with the previously published data.

TABLE III. Al₂O₃ ALD samples investigated by XPS, the used ALD parameters, and corresponding results. d is the Al₂O₃ thickness, Al:O the aluminium to oxygen ratio, and C the carbon content.

Sample	P _P W	P Pa	t _{TMA} s	t _{CR} s	t _{Purge} s/s	d nm	Al:O	C %
T-ALD (200 °C)	-	12	0.12	0.12	2/2	51	0.67	8.8
ICPEALD (250 °C)	200	12.8	0.06	15	5/1	104	0.62	10.6

For a detailed chemical analysis, the C1s core level spectra were decomposed. For this decomposition the Mg K α spectra were used because they exhibit a higher energy resolution than the Al K α data. The binding energy of the C1s main signal was calibrated to 284.5 eV; afterwards the spectra were decomposed into seven discrete peaks. The results for the T-ALD (200 °C) and ICPEALD (250 °C) samples are shown in Fig. 10. The most intense peak at 284.5 eV is attributed to covalent C–C and C–H bonds.²⁸ The peak located at 285.6 ± 0.1 eV points to C–O(H) species. The high binding energy region is satisfactorily fitted by three sub-peaks at 290.6 ± 0.2 eV, 289.1 ± 0.3 eV and 287.2 ± 0.2 eV, whose presence is attributed to various carbonate species.²⁹⁻³¹ The spectral weight of the carbonate sub-peaks is about 14 % for the ICPEALD (250 °C) sample whereas for the T-ALD (200 °C) sample it is 7.8 %. Typically, in PEALD combustion-like reactions accompanied by the formation of COO and H₂O³ may occur, which result in secondary reaction pathways⁴ and subsequently in the formation of carbonates and other types of carbon contamination. Furthermore, two sub-peaks at 283.2 ± 0.2 eV and 281.7 ± 0.3 eV are attributed to various carbide contributions,^{31,32} consistent with the formation of carbonaceous compounds containing elements with electronegativities lower than C

(2.55), e.g., Al (1.61). An extreme case is aluminum carbide (Al_4C_3) with its formal ionic charges of Al^{3+} and C^{4-} . Considering the significant, yet rather broad intensity in this region it is quite likely that in the films Al-C bonds are present, albeit not necessarily with the exact stoichiometry of Al_4C_3 . The ICPEALD (250 °C) sample shows a distinctly higher carbide spectral weight (36.6 %) than the T-ALD (200 °C) sample, whose carbide fractions amount to 17.7 %. Obviously, the relative abundance of carbide species varies with the preparation method and deposition parameters.

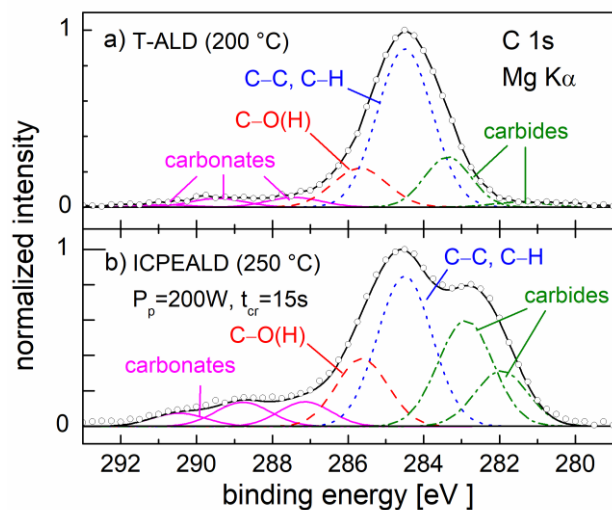


Fig. 10. Peak decomposition of the C1s core level spectra for differently prepared thin ALD films. a) T-ALD (200 °C), and b) ICPEALD (250 °C). The open black circles depicts the measured data while the nearby solid line represents the fitted data based on the sum of the peak components labeled in the diagram.

C. Discussion

In-situ real-time ellipsometry revealed an unintentional adsorption during ALD cycle Step #3 for longer plasma pulse durations as well as for higher plasma powers in

the ICPEALD process. This led to a decrease of TMA adsorption within the TMA pulse (refer to Figs. 3 and 4).

We interpret the unintentional adsorption during Step #3 of the ICPEALD cycle as a surface reaction induced by the plasma, which results in less nucleation centers on the surface. Thus, less TMA molecules can be adsorbed on the surface during the next TMA pulse (Step #1) of the next cycle. This effect is enhanced by a larger energy input and leads to additional carbon incorporation. This unintentional adsorption cannot be prevented by any variation in purge times (Step #2 and Step #4).

100 nm thick ICPEALD Al₂O₃ films with such an unintentional adsorption exhibit higher carbon concentration (10.6 %) and a lower Al:O ratio (0.62) in comparison to thick T-ALD deposited films (see Table III), consistent with an enhanced formation of carbonates (Fig. 10). These ICPEALD films also show a smaller Al-O LO stretching mode and additional absorption bands in the infrared ellipsometry spectra (Fig. 9) and a reduced spectral refractive index in the UV-VIS-NIR spectral range (Fig. 7). The decrease of the refractive index as a result of higher impurity levels is reported in the literature.¹³

IR spectra of ICPEALD films deposited at low plasma power ($P_p=50$ W, $t_{CR}= 15$ s) and short plasma pulses ($P_p= 200$ W, $t_{CR}= 1$ s) with higher deposition temperatures, e.g. 250 °C, exhibit only slightly lower Al-O LO stretching modes than T-ALD films. Also, the C-O and C-H modes are missing in the IR spectra of these ICPEALD films (see Fig. 9b). Still, the same strength of the Al-O LO stretching mode as in the T-ALD films could not be reached in these films, possibly indicating the presence of a slight number of oxygen defects within these films.

With increasing deposition temperature within the ICPEALD process, the concentration of Al atoms relative to oxygen concentration as well as the carbon concentration is reduced, in good agreement with literature.^{25,27} At lower deposition temperature, the TMA precursor interaction with the substrate is weak,²⁵ leading to a higher carbon content within the films.

For longer plasma pulse times, the Al-O mode is also weakened (Fig. 9a) but the GPC values are not increased (Fig. 8a). In this case, a temperature dependence of the GPC was not observed in contrast to the films prepared with short plasma pulse duration. The Al-O stretching mode was equally reduced for higher and lower temperatures when the plasma pulse was prolonged. Thus, a different incorporation must be the reason.

In our experiments, the refractive index change is not reflected in a change of GPC. Figure 8 illustrates a GPC that remains unaffected by the drop of the refractive index for longer plasma pulses but decreased for increased refractive index at shorter plasma pulses (see Figs. 8a and 8c). Roughly, the same GPC values were reached for high deposition temperature (250 °C) with lower plasma power pulses ($P_p=50$ W, $t_{CR}=15$ s), high power and reduced pulse time and ($P_p=200$ W, $t_{CR}=1$ s) as well as high power and long plasma pulse ($P_p=200$ W, $t_{CR}=15$ s) (compare Fig. 8a). But, the refractive index varied drastically for these films (see Fig. 8c). Hence, the comparison of the GPC of different processes is not sufficient to characterize the quality of the film; rather the film density should also be investigated.³³

The onset of UV-VIS absorption is at three different levels (compare Figure 8 b). The T-ALD film has an absorption onset of ~ 210 nm. Those ICPEALD films with the unintentional adsorption (in Step #3, see above) reveal a late onset around 300 nm. Yet,

ICPEALD films with refractive indexes and Al-O LO stretching intensities comparable to T-ALD films show a very early onset at ~ 500 nm, in strong contrast to the onset of the T-ALD films. The mentioned ICPEALD films have no carbon based absorption bands in the infrared spectral region, as discussed above (Fig. 9b). Thus, an early onset of absorption at 500 nm does not correlate with impurities.

Absorption losses in the UV-VIS spectral range can be caused by stoichiometry variations and oxygen deficiencies³⁴ (although impurities have been minimized), as reported for electron beam evaporated films in Ref. 35. Although, our films are amorphous, we follow the argumentation of Heber et al. about oxygen vacancies with one trapped electron (F^-). These high purity Al_2O_3 films showed an emission center around 400 nm and an onset of absorption at ~ 500 nm.³⁵ This explains the abovementioned UV-VIS absorption of the ICPEALD films and the fact that its Al-O LO stretching is not as strong as for the T-ALD films. It might also explain the small increase in $\delta\Delta$ for Step #3 of short plasma lengths (e.g. $t_{CR} = 1$ s) deposited films in Fig. 5a. More oxygen is incorporated in the film for higher temperatures and shorter plasma pulse lengths or lower power during the O_2 plasma pulse (particularly for $P_p=200$ W, $t_{CR}=1$ s as well as $P_p=50$ W, $t_{CR}=15$ s, 50 W, refer to Figs. 5a and 5c, respectively). Further analysis, such as density, stress, and photoluminescence measurements, is required to confirm oxygen deficiencies as the reason for UV-absorption in the ICPEALD deposited Al_2O_3 films.

Thus, the application of in-situ real-time ellipsometry enabled the detection of impurities and carbon incorporation already during the ALD cycle process steps. In addition, some sensitivity to even smallest amounts of oxygen deficiencies was demonstrated.

IV. SUMMARY

The influence of plasma power and deposition temperature was investigated for plasma enhanced atomic layer deposition of Al₂O₃ films using an inductively coupled plasma source. The in-situ analysis of ad- and desorption during each cycle of the ICPEALD showed characteristic deviations compared to T-ALD using water vapor for the oxidation step. Particularly, these ad- and desorption processes were demonstrated to be dependent on the oxygen plasma power and oxygen plasma pulse duration. The observed deviations were mainly due to kinetic surface processes caused by the high ion flux of the ICP plasma source and highly energetic particles such as ions and photons. The subsequent ex-situ analysis of the film properties showed increased carbon incorporation with increasing plasma power and pulse time, resulting in nonstoichiometric films with lower refractive index and increased absorption in the UV-VIS spectral range. High temperature and high-power deposition revealed the formation of aluminum carbides, which were responsible for the strong decrease of the refractive index in the entire spectral range.

In summary, by applying real-time monitoring during each ALD cycle, the ICP pulse time and power can be quickly and easily adjusted. Monitoring the process allows adjustments that minimize kinetic effects during plasma operation. As a consequence, ICPEALD Al₂O₃ films with comparable optical properties and chemical composition as T-ALD Al₂O₃ films can be achieved.

ACKNOWLEDGMENTS

The XPS investigations were funded by the Federal Ministry for Economic Affairs and Energy (BMWi) of Germany within the ZIM program (ZF4245503AG7, ZF4510602AG7). A. Mahmoodinezhad acknowledges the funding by the Graduate Research School of Brandenburg University of Technology Cottbus-Senftenberg within the cluster 'Functional Materials and Film Systems for Efficient Energy Conversion (FuSion)'.

¹M. Knez, K. Nielsch, and L. Niinistö, *Adv. Mater.* **19**, 3425 (2007).

²S. M. George, *Chem. Rev.* **110**, 111 (2010).

³G. Dingemans and W. M. M. Kessels, *J. Vac. Sic. Technol. A* **30**, 040802 (2012).

⁴H. B. Profijt, S. E. Potts, M. C. M. van de Sanden, and W. M. M. Kessels, *J. Vac. Sci. Technol. A* **29**, 050801 (2011).

⁵M. Tallarida and Dieter Schmeisser, *Semicond. Sci. Technol.* **27**, 074010 (2012).

⁶K. Kolanek, M. Tallarida, M. Michling, K. Karavaev, and D. Schmeißer, *Phys. Status Solidi C* **8**, 1287 (2011).

⁷S. Sarkar, J. H. Culp, J. T. Whyland, M. Garvan, and V. Misra, *Org. Electron.* **11**, 1896 (2010).

⁸K. Henkel, M. Torche, R. Sohal, K. Karavaev, Y. Burkov, C. Schwiertz, and D. Schmeißer, *Phys. Status Solidi A* **208**, 317 (2011).

⁹M. Cho et al., *J. Appl. Phys.* **94**, 2563 (2003).

- ¹⁰K. Henkel, B. Seime, I. Paloumpa, K. Mueller, and D. Schmeißer, IOP Conf. Series: Mater. Sci. Eng. **8**, 012036 (2010).
- ¹¹M. Tallarida, M. Weisheit, K. Kolanek, M. Michling, H.-J. Engelmann, and D. Schmeißer, J. Nanopart. Res. **13**, 5975 (2011).
- ¹²M. Tallarida, K. Kukli, M. Michling, M. Ritala, M. Leskela, and D. Schmeißer, Chem. Mater. **23**, 3159 (2011).
- ¹³M. D. Groner, F. H. Fabreguette, J. W. Elam, and S. M. George, Chem. Mater. **16**, 639 (2004).
- ¹⁴F. Speck, M. Ostler, J. Röhr, K. V. Emtsev, M. Hundhausen, L. Ley, and T. Seyller, Phys. Status Solidi C **7**, 398 (2010).
- ¹⁵Q. Peng, J. S. Lewis, P. G. Hoertz, J. T. Glass, and G. N. Parsons, J. Vac. Sci. Technol. A **30**, 010803 (2012).
- ¹⁶C. Prasittichai and J. T. Hupp, J. Phys. Chem. Lett. **1**, 1611 (2010).
- ¹⁷T.-C. Tien, F.-M. Pan, L.-P. Wang, F.-Y. Tsai, and C. Lin, J. Phys. Chem. C **114**, 10048 (2010)
- ¹⁸F. Le Formal, N. Tétreault, M. Cornuz, T. Moehl, M. Gratzel, and K. Sivula, Chem. Sci. **2**, 737 (2011).
- ¹⁹Y. S. Jung, A. S. Cavanagh, A. C. Dillon, M. D. Groner, S. M. George, and S. H. Lee, J. Electrochem. Soc. **157**, A75 (2010).
- ²⁰ M. Kot, C. Das, K. Henkel, K. Wojciechowski, H. J. Snaith, D. Schmeisser, Nucl. Instrum. Methods Phys. Res., Sect. B **411**, 49 (2017)

- ²¹S. B. S. Heil, P. Kudlacek, E. Langereis, R. Engeln, M. C. M. van de Sanden, and W. M. M. Kessels, *Appl. Phys. Lett.* **89**, 131505 (2006).
- ²²K. Henkel, H. Gargouri, B. Gruska, M. Arens, M. Tallarida, and D. Schmeißer, *J. Vac. Sci. Technol. A* **32**, 01A1071 (2014).
- ²³G. Blasik, G. Bräuer et al., *Vakuum Plasma Technologien*, (EUGEN LEUZE VERLAG KG, Bad Saulgau, 2010), K. Wandel, pp 451.
- ²⁴G.E. Jellison Jr., F.A. Modine, P. Doshi, A. Rohatgi, *Thin Solid Films*, **313-314**, (1998).
- ²⁵P. Ruffieux, P. Schwaller, O. Gröning, L. Schlapbach, and P. Gröning, *Rev. Sci. Instrum.* **71**, 3634 (2000).
- ²⁶R. Puurunen, *J. Appl. Phys.* **97** 121301 (2005).
- ²⁷J. Haeberle, K. Henkel, H. Gargouri, F. Naumann, B. Gruska, M. Arens, M. Tallarida, and D. Schmeißer, *Beilstein J Nanotechnol.* **4**, 732 (2013).
- ²⁸K. Fröhlich, M. Mičušík, E. Dobročka, P. Šiffalovič, F. Guemann, J. Fedor, Properties of Al₂O₃ thin films grown by atomic layer deposition, in: *The Ninth International Conference on Advanced Semiconductor Devices and Microsystems*, (IEEE Smolenice, Slovakia, 2012) pp. 171-174.
- ²⁹A. Dolgov, D. Lopaev, C.J. Lee, E. Zoethout, V. Medvedev, O. Yakushev, and F. Bijkerk, *Appl. Surf. Sci.* **353**, 708 (2015).
- ³⁰A. Shchukarev and D. Korolkov, *D. Open Chem.* **2**, 347 (2004).
- ³¹J.F. Moulder, W.F. Stickle, P.E. Sobol, and K.D. Bomben, In J. Chastain and R.C. King, Jr. (Eds) *Hand book of X-ray Photoelectron Spectroscopy. A Reference Book of*

This is the author's peer reviewed, accepted manuscript. However, the online version of record will be different from this version once it has been copyedited and typeset.
PLEASE CITE THIS ARTICLE AS DOI: 10.1116/1.5122797

Standard Spectra for Identification and Interpretation of XPS Data, (Physical Electronics Inc., Eden Prairie, Minnesota, 1995).

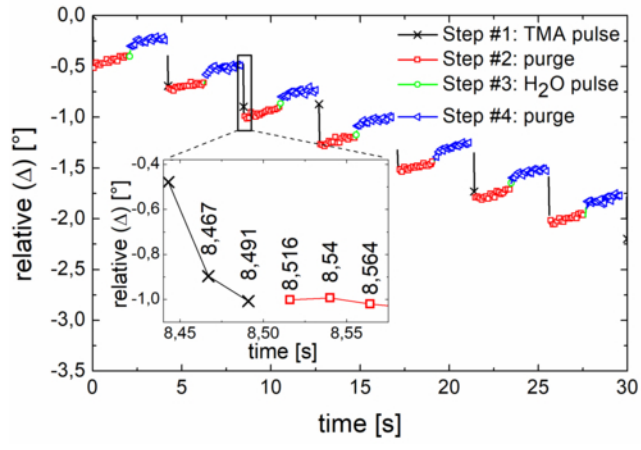
³²N. Nedfors, O. Tengstrand, A. Flink, A. M. Andersson, P. Eklund, L. Hultman, and U. Jansson, Surf. Coat. Technol. **253**, 100 (2014).

³³Z. Zhu, P. Sippola, H. Lipsanen, H. Savin, S. Merdes, Jpn. J. Appl. Phys. **57**, 125502 (2018).

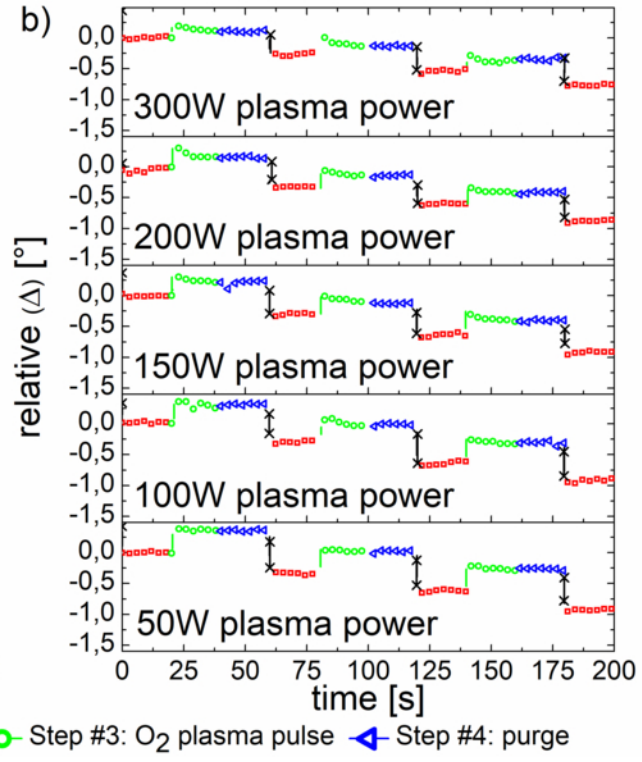
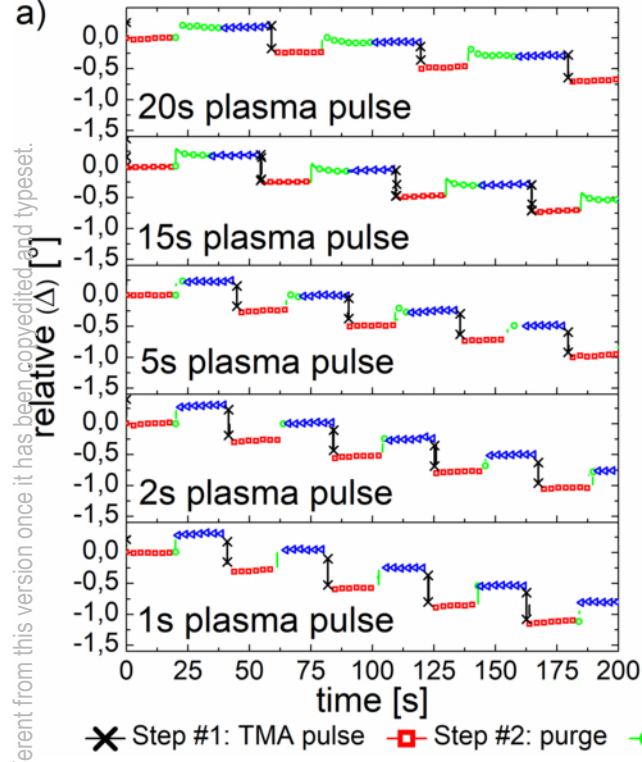
³⁴O. Stenzel, S. Wilbrandt, S. Du, C. Franke, N. Kaiser, A. Tünnermann, M. Mende, H. Ehlers, M. Held, Optical Materials Express, **4**, 8 (2014).

³⁵J. Heber, C. Mühlig, W. Triebel, N. Danz, R. Thielsch, N. Kaiser, Appl. Phys. A **75**, 637 (2002).

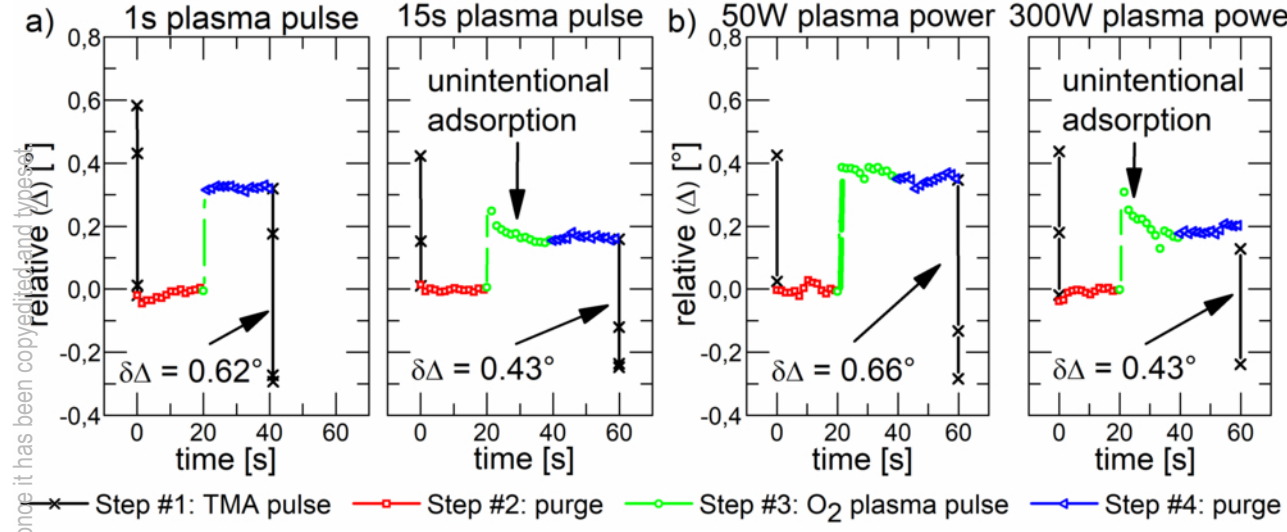
This is the author's peer reviewed, accepted manuscript. However, the online version of record will be different from this version once it has been copyedited and typeset.
PLEASE CITE THIS ARTICLE AS DOI: 10.1116/1.5122797



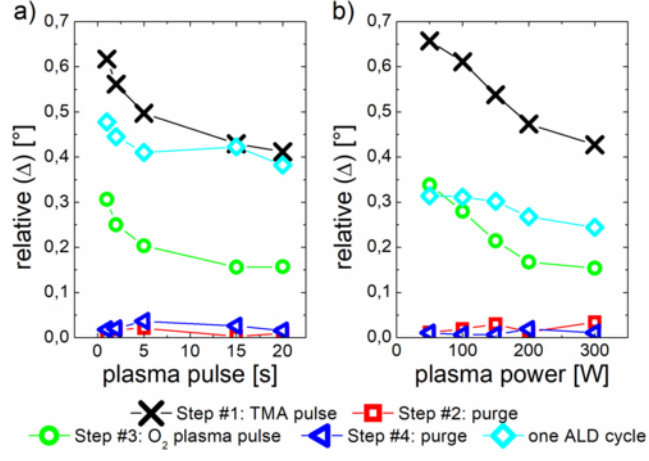
This is the author's peer reviewed, accepted manuscript. However, the online version of record will be different from this version once it has been copyedited and typeset.
PLEASE CITE THIS ARTICLE AS DOI: 10.1116/1.5122797



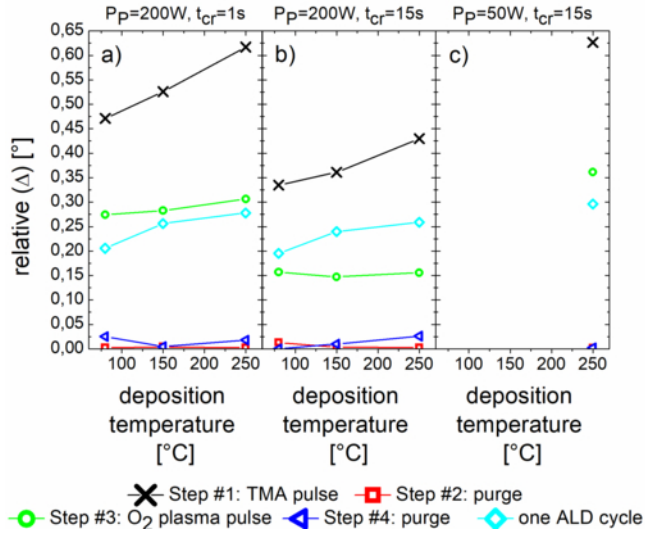
This is the author's peer reviewed, accepted manuscript. However, the online version of record will be different from this version once it has been copyedited and typeset.
PLEASE CITE THIS ARTICLE AS DOI: 10.1116/1.5122797



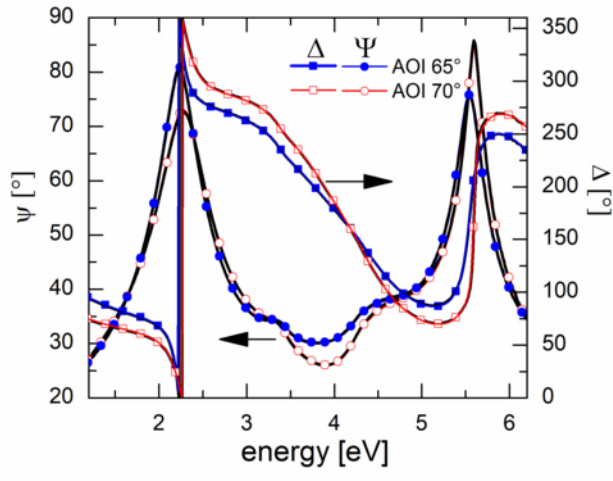
This is the author's peer reviewed, accepted manuscript. However, the online version of record will be different from this version once it has been copyedited and typeset.
PLEASE CITE THIS ARTICLE AS DOI: 10.1116/1.5122797



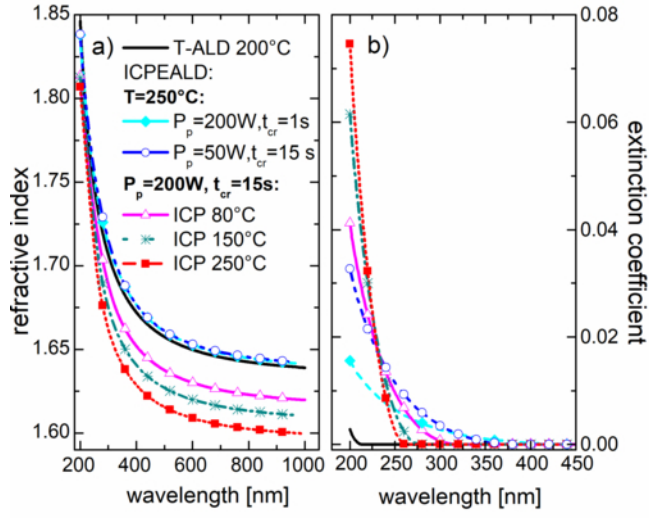
This is the author's peer reviewed, accepted manuscript. However, the online version of record will be different from this version once it has been copyedited and typeset.
PLEASE CITE THIS ARTICLE AS DOI: 10.1116/1.5122797



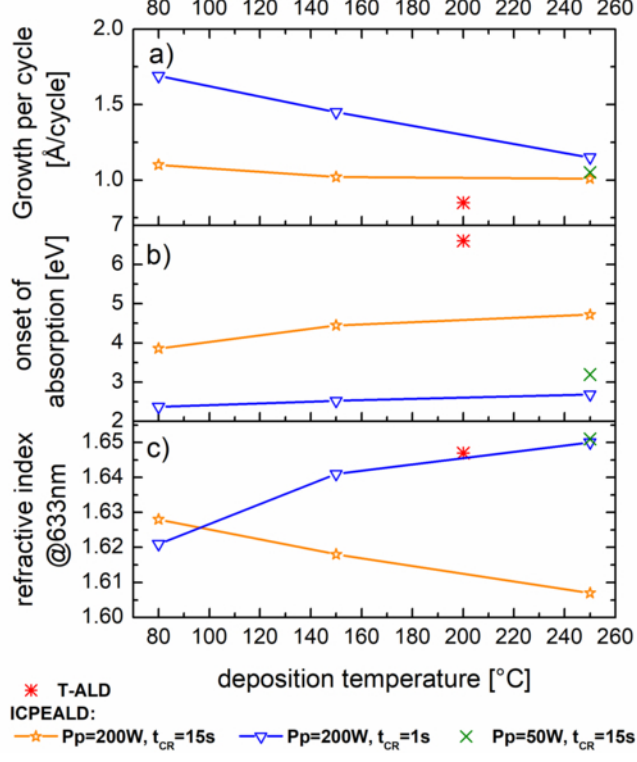
This is the author's peer reviewed, accepted manuscript. However, the online version of record will be different from this version once it has been copyedited and typeset.
PLEASE CITE THIS ARTICLE AS DOI: 10.1116/1.5122797



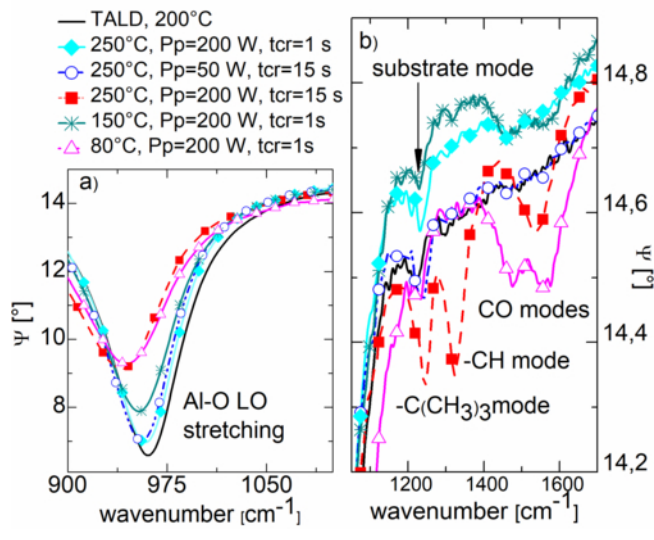
This is the author's peer reviewed, accepted manuscript. However, the online version of record will be different from this version once it has been copyedited and typeset.
PLEASE CITE THIS ARTICLE AS DOI: 10.1116/1.5122797



This is the author's peer reviewed, accepted manuscript. However, the online version of record will be different from this version once it has been copyedited and typeset.
PLEASE CITE THIS ARTICLE AS DOI: 10.1116/1.5122797



This is the author's peer reviewed, accepted manuscript. However, the online version of record will be different from this version once it has been copyedited and typeset.
PLEASE CITE THIS ARTICLE AS DOI: 10.1116/1.5122797



This is the author's peer reviewed, accepted manuscript. However, the online version of record will be different from this version once it has been copyedited and typeset.
PLEASE CITE THIS ARTICLE AS DOI: 10.1116/1.5122797

